

Phase Transition of Gd_3RuO_7 from a Structural Point of View

H. Nakano[†], K. Tateishi[‡], and N. Ishizawa[¶]

[†] Ryukoku University, Seta, Otsu 520-2194

[‡] Gifu Prefectural Ceramics Research Institute, Hoshigadai, Tajimi 507-0811

[¶] Ceramics Research Laboratory, Nagoya Institute of Technology, Asahigaoka, Tajimi 507-0071

構造的観点からみた Gd_3RuO_7 の相転移

中野裕美[†]・立石賢司[‡]・石澤伸夫[¶]

[†] 龍谷大学 〒 520-2194 滋賀県大津市瀬田大江町横谷 1-5

[‡] 岐阜県セラミックス研究所 〒 507-0811 多治見市星ヶ台 3-11

[¶] 名古屋工業大学セラミックス基盤工学研究センター 〒 507-0071 岐阜県多治見市旭ヶ丘 10-6-29

Gd_3RuO_7 , the ordered oxygen-deficient fluorite-type compound, undergoes a structural phase transition between the $P2_1nb$ and $Cmcm$ modifications at around 382 K. This paper describes the phase transition from a structural point of view, based on the high-temperature single-crystal X-ray and electron diffraction studies. The transition is almost reversible, and characterized by an additional tilt about the c axis that occurs in the low-temperature modification for half of the RuO_6 octahedra in association with a reduction of apparent coordination number from 6+2 to 7 for one-third of Gd atoms. Dimerization of the Ru array along the $[-RuO_5]_{\infty}$ zigzagging chain occurs below the transition temperature, which provides a folding effect on the chain. The folding tendency of the chain explains geometrically an expansion of the b -length and a compression of the c -length near 382 K on cooling and *vice versa* on heating. The transition is similar to those given in the literature for Sm_3RuO_7 , Eu_3RuO_7 , Sm_3OsO_7 , Eu_3OsO_7 and Gd_3OsO_7 , except that one of crystallographically independent Gd atoms in the high-temperature $Cmcm$ modification is statically or dynamically distributed between two positions located very close with each other. The disordered distribution of the Gd atom in the high-temperature modification is presumably correlated with the octahedral tilts about the c axis, resulting in the experimental observation of the extremely prolate atomic displacement ellipsoid for the O1 atom in the *cis* position along the chain. The $P2_1nb$ - $Cmcm$ phase transition contains two competing mechanisms characterized by the order-disorder transition of the librating $[-Gd-RuO_6-Gd-RuO_6-Gd-]$ linkage along the b axis, and by the displacive-type dimerization of Ru atoms along the chain. The *in situ* electron diffraction experiments suggested a possible existence of intermediate phase between the high- and low-temperature modifications.

1. Introduction

Compounds of the Ln_3MO_7 series are composed of trivalent lanthanide (Ln) and pentavalent transition metal oxides and crystallizes in the defect-fluorite-type structure (Allpress & Rossel, 1979). The structure was first determined for La_3NbO_7 on the basis of the $Cmcm$ symmetry. Among the Ln_3MO_7 series, Ln_3RuO_7 and Ln_3OsO_7 contain the MO_6 octahedral single-chains in the matrix composed of

Ln and O atoms. The unit-cell relationship between the cubic fluorite-type parent structure (f) and the Gd_3RuO_7 -type chain structure (c) is shown in Fig. 1. The crystals show the polymorphism. The phase transition between the space groups $P2_1nb$ and $Cmcm$ was first reported for Sm_3RuO_7 at 190 K, and Eu_3RuO_7 at 280 K (Gemmill *et al.*, 2004), and then for Sm_3OsO_7 at 235 K, Eu_3OsO_7 at 330 K, and Gd_3OsO_7 at 430 K (Gemmill *et al.*, 2005).

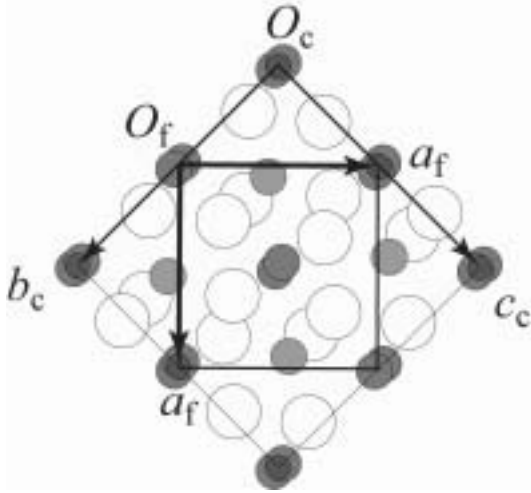


Fig. 1. The unit-cell relationship between the cubic fluorite-type parent structure (f) and the Gd_3RuO_7 -type chain structure (c). Metal and oxygen atoms are represented by filled and unfilled circles, respectively.

The $Cmcm$ structure is considered as archetypal, possessing the highest symmetry among the Ln_3RuO_7 polymorphs.

Bontchev *et al.* (2000) grew single crystals of Gd_3RuO_7 by the flux method and suggested that the crystal has localized carriers in one-dimension with Mott variable range hopping along the octahedral single chains. They also reported two phase transitions at 14.5 and 8 K relevant to the orderings of the Ru and Gd magnetic moments, respectively. Harada & Hinatsu (2002) found another transition at 382 K for Gd_3RuO_7 and reported from the specific heat measurement that the transition is of the first order.

The room temperature structure of Gd_3RuO_7 was first analyzed also assuming $Cmcm$, which made ourselves difficult to presume the symmetry of the high-temperature modification of Gd_3RuO_7 above 382 K. Recently, the crystal structure of Gd_3RuO_7

at room temperature was reexamined and found to possess the $P2_1nb$ symmetry (Ishizawa *et al.*, 2006). The phase transition of Gd_3RuO_7 between $P2_1nb$ and $Cmcm$ was then detailed by the *in situ* single-crystal X-ray diffraction study (Ishizawa *et al.*, 2007). The present paper aims at filling up the unreported things which were excluded from our past papers mainly due to the space problems, and to discuss the nature of the phase transition of Gd_3RuO_7 from a structural point of view. This paper also includes a latest finding about the possible presence of intermediate phase near the phase transition obtained from the electron microscopy study.

2. Crystal shape and its relation to the structure

Crystals were grown by cooling the $\text{SrCl}_2\text{-RuO}_2\text{-Gd}_2\text{O}_3$ solution at the rate of 5 Kmin^{-1} from 1373 K. Experimental details are given in our previous papers (Ishizawa *et al.*, 2006, 2007). Metallic black crystals had a prismatic shape surrounded by $\{120\}$ side faces and capped by $\{101\}$. As shown in Fig. 2, these faces correspond to the planes extending through the crystal so that they can avoid strong bonds between the pentavalent Ru cation and the divalent oxide anions. The RuO_6 octahedral chains are running along the c axis which corresponds to the columnar direction of the as-grown crystal. Therefore it is not difficult to distinguish the direction of the maximum electric conduction for the crystals in columnar shape.

3. Choice of space group

Precession images were reconstructed from the frame data taken by the CCD single-crystal diffractometer (Smart Apex II, Bruker) at various temperatures between 293 to 1223 K. The $0kl$ planes at 423 K and 293 K are shown in Fig. 3. In the high-temperature modification, only the reflections with $k=\text{even}$ were observed due to the lattice centering.

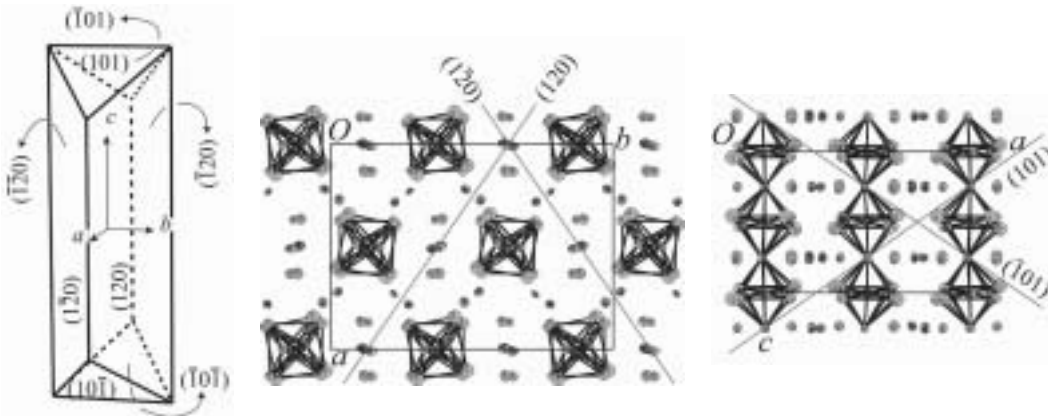


Fig. 2. Face indices of a typical as-grown crystal and their relation to structure.

In the low-temperature modification, on the other hand, satellite reflections at both sides of parent reflections appear along the b axis. The satellites are commensurate and can be indexed by doubling the b -length. The lattice loses the centering and becomes primitive.

Intensity data of the low-temperature modification were collected at 293 K up to $d=0.40$ Å resolution level ($2\theta < 124^\circ$ for Mo $K\alpha$) by the CCD diffractometer. Those of the high-temperature modification were collected at 423, 773 and 1223 K. Crystal data are given in Table 1. Numerical details have been given by Ishizawa *et al.*, (2007). The agreement index for the intensities of crystallographically equivalent reflections, R_{merge} , in the low-temperature modification showed no significant improvement by reducing the Laue symmetry from mmm to lower ones. The crystal was thus assumed to have an orthorhombic symmetry. From the systematic absence of reflections, possible space groups were limited to $P2_1nb$ and $Pmnb$. The noncentrosymmetric $P2_1nb$ was adopted because the mirror planes perpendicular to the a axis in the centrosymmetric $Pmnb$ did not allow octahedral tilts about the axes on the planes.

Figure 4 shows the temperature dependence of the mean $|Fo|^2$ of eight reflection parity groups, $eo\bar{e}$, ooo , ooe , $eo\bar{o}$, $0oo$, $0oe$, $o0\bar{o}$ and $e0\bar{o}$, on the basis of the $P2_1nb$ lattice. The reflections in these groups can exist in $P2_1nb$ and should disappear in $Cmcm$. The data were collected upon heating. The temperature dependence was essentially the same on cooling the specimen, suggesting that the transition is almost reversible. The mean $|Fo|^2$ of the first seven parity groups, *i.e.*, $eo\bar{e}$, ooo , ooe , $eo\bar{o}$, $0oo$, $0oe$ and $o0\bar{o}$, decreased rapidly with increasing temperature and disappeared above 382 K. The reflections of the parity group $e0\bar{o}$ were slightly stronger and more diffuse than those of the other seven groups above 382K, although the $|Fo|^2$ value of the strongest

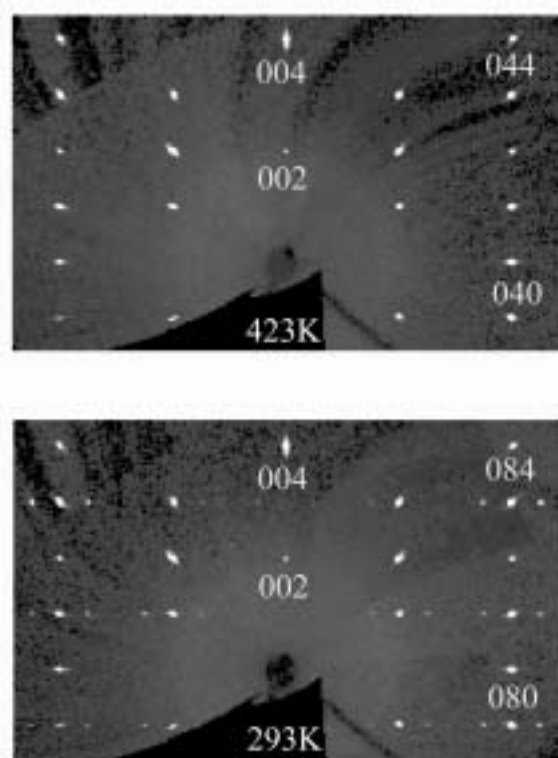


Fig. 3. Precession images of the reciprocal $0kl$ plane at 423 K ($Cmcm$) and 293 K ($P2_1nb$), calculated from the CCD frame data.

reflection in the group $e0\bar{o}$ did not exceed 3 times its estimated standard uncertainty. They were thus neglected for the space group determination.

Some of the Ln_3MO_7 crystals, *e.g.*, Ln_3MO_7 ($M=\text{Nb}$, Ta and Sb , $\text{Ln}=\text{Nd}$, Gd and Ho) (Allpress & Rossel, 1979), Y_3TaO_7 (Rossel, 1979), and Dy_3ReO_7 (Hinatsu *et al.*, 2004), have been reported to crystallize in the space group $C222_1$. The space groups of $C222_1$ and $Cmcm$ can be distinguished from the $h0l$ reflections, *i.e.*, the reflection group $e0\bar{o}$

Table 1. Crystallographic Data for Gd_3RuO_7

formula	Gd_3RuO_7	Gd_3RuO_7	Gd_3RuO_7	Gd_3RuO_7
fw (g/mol)	684.82	684.82	684.82	684.82
temperature (K)	293	423	773	1223
wavelength (Å)	0.71073	0.71073	0.71073	0.71073
crystal system	orthorhombic	orthorhombic	orthorhombic	orthorhombic
space group	$P2_1nb$	$Cmcm$	$Cmcm$	$Cmcm$
unit cell dimensions				
a (Å)	10.6399(2)	10.6514(2)	10.6847(2)	10.7346(2)
b (Å)	14.6769(2)	7.3404(3)	7.3694 (1)	7.4112(2)
c (Å)	7.3747 (1)	7.3942 (1)	7.4136 (1)	7.4481(2)
volume (Å ³)	1151.64(3)	578.12(3)	583.75(2)	592.54(3)
Z	8	4	4	4

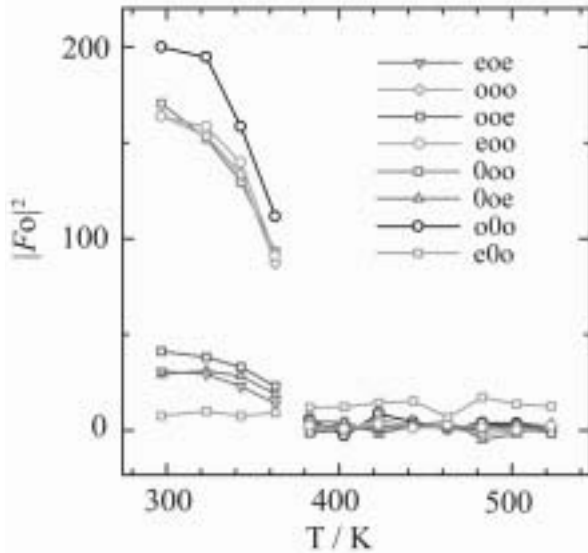


Fig. 4. Temperature dependence of the mean $|F_o|^2$ of seven reflection parity groups, eoe, ooo, ooe, eoo, 0oo, 0oe, o0o and e0o, where o and e stands for odd and even indices, respectively, on the basis of the $P2_1nb$ lattice. The data points are connected by polylines in the high- and low-temperature modifications for viewing purpose.

are allowed for $C222_1$ whereas not for $Cmcm$. The possibility of $C222_1$ was discarded for this crystal by the aforementioned reason in the present study.

4. Changes in the cell dimensions

Temperature dependences of the cell dimensions in the range between 293 K and 523 K are shown in Fig. 5. A small shrinkage of the b -length and an expansion of the c -length were observed between the 363 and 383 K data points upon heating and the reverse took place upon cooling. Between these data points lies the phase transition temperature of 382 K reported from the specific heat measurement. The changes in the cell dimensions suggest that the transition is almost reversible. The a -length changed

monotonically and no anomaly was observed within experimental errors.

5. Octahedral tilts and distortion

The structures of the high- and low-temperature modifications are illustrated in Fig. 6. There are two crystallographically independent octahedra, RuO_6 and Ru_2O_6 in the low-temperature $P2_1nb$ modification. The two octahedra alternate along the c axis by sharing the *trans* O3 atom (O_t) to form a zigzagging single chain of $[-\text{RuO}_5-\text{Ru}_2\text{O}_5-]_\infty$. These single chains are embedded and separated with each other in a matrix consisting of Gd and O atoms. The RuO_6 octahedron has practically one tilt system about an axis parallel to the a axis. On the other hand, the Ru_2O_6 octahedron has a second tilt system about an axis parallel to the c axis in addition to the first tilt about the axis parallel to a .

The two independent RuO_6 and Ru_2O_6 octahedra in the $P2_1nb$ modification become crystallographically identical in $Cmcm$. The RuO_6 in the high-temperature modification has a single tilt system about a . The appearance and disappearance of the tilt about c for every other RuO_6 octahedra is a structural feature that characterizes the $P2_1nb$ - $Cmcm$ phase transition.

Several important geometrical parameters obtained from the least-squares procedure are listed in Table 2. The RuO_6 octahedra are elongated along the chain in the high-temperature modification as seen from the ratio of $\langle \text{Ru-O}_t \rangle_2 / \langle \text{Ru-O}_c \rangle_4$, where O_c stands for the O1 atom in the *cis* position of octahedra with respect to O_t , and the angle brackets stand for taking an average over the number of bonds given as a subscript. The values of quadratic elongation and angle distortion in Table 2 suggest that the shape of oxygen octahedra in the high-temperature modification resolves into more distorted RuO_6 and less distorted Ru_2O_6 in the low-temperature modification (Robinson *et al.*, 1971). The Ru-O_t - Ru angle of 142.5° at 423 K is slightly more obtuse

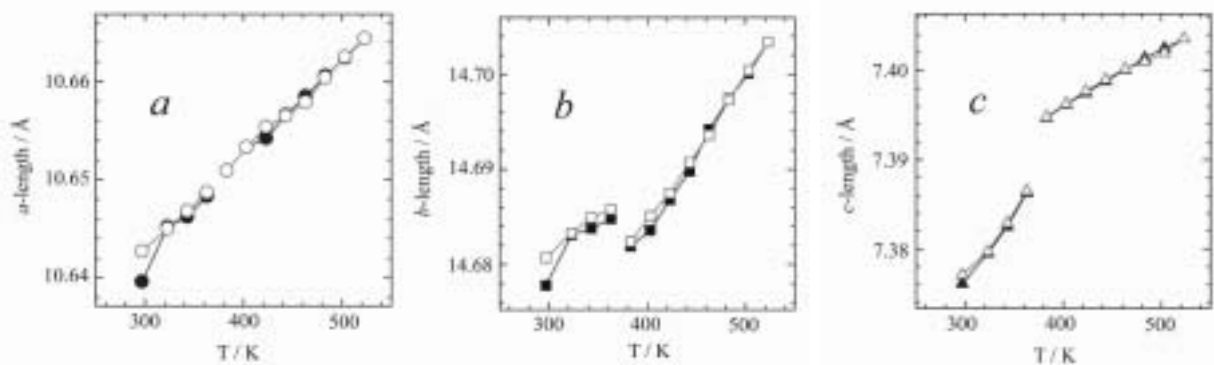


Fig. 5. Temperature dependence of the a -, b -, and c -lengths of Gd_3RuO_7 . Data points of filled black marks on heating and open red ones on cooling are connected by polylines for viewing purpose. The b -length of the $Cmcm$ modification above 382 K is doubled in the figure for comparison with the low-temperature $P2_1nb$ modification. The estimated standard uncertainties of the cell lengths are less than the marker size.

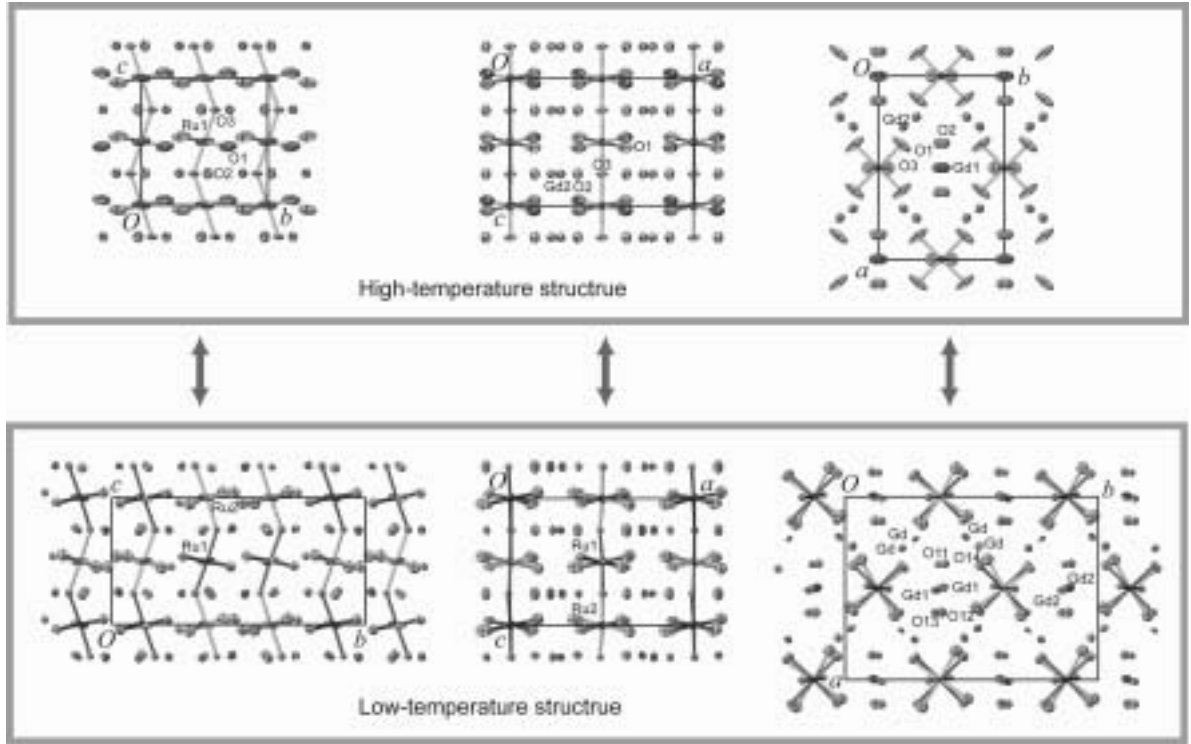


Fig. 6. Comparison of the high- and low-temperature modifications at 423 K and 293 K with atomic displacement parameter ellipsoids plotted at the 97% probability level.

Table 2. Selected interatomic distances (\AA) and geometry parameters

	293 K		423 K	773 K	1223 K
$\langle \text{Ru1-O} \rangle_6$ (\AA)	1.947(8)		1.945(2)	1.953(4)	1.948(4)
$\langle \text{Ru1-O}_t \rangle_2$ (\AA)	1.945(8)		1.952(1)	1.959(2)	1.967(2)
$\langle \text{Ru1-O}_c \rangle_4$ (\AA)	1.948(6)		1.941(2)	1.950(4)	1.949(4)
$\langle \text{Ru1-O}_t \rangle_2 / \langle \text{Ru1-O}_c \rangle_4$	0.9985		1.0057	1.0046	1.0092
Octahedral volume (\AA^3)	9.744		9.738	9.857	9.897
Quadratic elongation	1.006		1.005	1.005	1.005
Angle variance	22.85		16.94	18.65	16.78
$\langle \text{Ru2-O} \rangle_6$ (\AA)	1.949(7)				
$\langle \text{Ru2-O}_t \rangle_2$ (\AA)	1.953(6)				
$\langle \text{Ru2-O}_c \rangle_4$ (\AA)	1.947(8)				
$\langle \text{Ru1-O}_t \rangle_2 / \langle \text{Ru1-O}_c \rangle_4$	1.0031				
Octahedral volume (\AA^3)	9.807				
Quadratic elongation	1.004				
Angle variance	14.63				
$\text{Ru1} \cdots \text{Ru2}$ (\AA)	3.683(4), 3.691(4)	$\text{Ru1} \cdots \text{Ru1}$ (\AA)	3.6971(1)	3.7068(1)	3.7241(1)
Ru1-O1-Ru2 angle ($^\circ$)	140.4(5)	Ru-O3-Ru angle ($^\circ$)	142.5(2)	142.2(4)	142.4(4)
Ru1-O2-Ru2 angle ($^\circ$)	144.1(5)				

^a The interatomic distances (\AA) in angle brackets are the average over the shortest n bonds with n given as a subscript. The O_t represents *trans* O atoms connecting the RuO_6 octahedra along the chain, and O_c represents the other *cis* O atoms of RuO_6 octahedra.

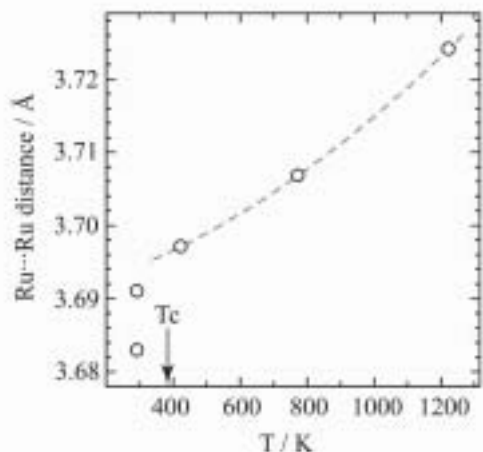


Fig. 7. Changes in the intermetallic Ru··Ru distance along the RuO_6 chain with temperature. The estimated standard uncertainties are within the marker size. Two Ru··Ru distances in the $P2_1nb$ modification at 293 K lie below the dashed quadratic polynomial line connecting the values in the $Cmcm$ modification at high temperatures.

than the mean of the two $\text{Ru-O}_7\text{-Ru}$ angles at 293K in the low-temperature modification, *i. e.*, $140.4(5)^\circ$ for Ru1-O1-Ru2 and $144.1(5)^\circ$ for Ru1-O2-Ru2 . This indicates that the octahedral single chain tends to unfold in the high-temperature modification.

6. Ru··Ru intermetallic distance

Along the chain, there is one kind of intermetallic Ru··Ru distance in the high-temperature modification, corresponding to the half of the c length, whereas there are two kinds of Ru··Ru distances in the low-temperature modification. The temperature dependence of the Ru··Ru distance is shown in Fig. 7. The Ru··Ru distance in the high-

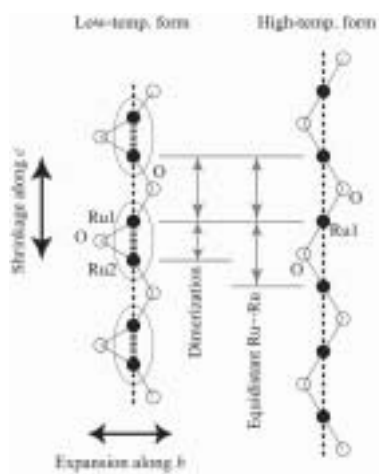


Fig. 8. Schematic drawing of the RuO_6 chain featuring the relation between the dimerization of Ru atoms and the changes of cell dimensions on the transition.

temperature modification is much larger than their mean in the low-temperature modification. The elongation of octahedra, the unfolding tendency of the chain, and the increase of intermetallic Ru··Ru distance accord geometrically with each other. They also explain the shrinkage of the b -length and the expansion of the c -length (Fig. 5) near the phase transition point upon heating and *vice versa* upon cooling. The inequality of Ru··Ru intermetallic distances along the chain in the low temperature modification (Fig. 7) indicates that the dimerization of adjacent Ru atom pairs takes place in addition to the general shortening of the Ru··Ru distances. This suggests a higher, and slightly different, electronic correlation between the Ru atoms along the chain in the low-temperature modification compared with the high-temperature one. A detailed analysis of the band structure is necessary in order to understand the phase transition as well as the conduction properties.

7. Dynamic disorder in the high-temperature modification

The RuO_6 octahedral single chains are bridged with each other along the b axis by the Gd1-O1 bonds, as shown in Fig. 9. The bridging is symmetrical in the high-temperature modification due to the presence of mirror planes perpendicular to the a axis. The presence of mirrors prevents octahedral tilting about c . Below the transition temperature, each Gd1 atom releases one bond to RuO_6 octahedron, enabling a tilt about c for every other RuO_6 octahedra. This is essentially the same as those reported for the $P2_1nb$ - $Cmcm$ phase transitions in Sm_3RuO_7 and Eu_3RuO_7 , Sm_3OsO_7 , Eu_3OsO_7 and Gd_3OsO_7 .

The $Cmcm$ structures determined at 423, 773 and 1223 K are shown in Fig. 10. The distance of the Gd atom split pair was approximately 0.3 Å, and did not show any significant temperature dependence. The atomic displacement parameters increased almost linearly as a function of temperature. It is notable that only the O1 atom in *cis* position has an extremely prolate atomic displacement parameter ellipsoid, as the overlapped Gd1 split pair looks like in Fig. 9.

The coordination geometry around Gd1 can be modified depending on the actual Gd1 atom location in the split pair. Figure 11 illustrates four possible geometries in the high-temperature modification. The directions of Gd1 atom shifts are the same in (a) and (b), and are reversed in (c) and (d). The Gd1 atom is coordinated by two O_c atoms of an octahedron by occupying a closer position to the octahedron. On the other hand, the shift provides to the other adjacent octahedron one of the two possible tilts (clockwise or counterclockwise) about the axes close to c , by releasing one Gd1-O_c bond. Depending on the directions of Gd1 atom shifts,

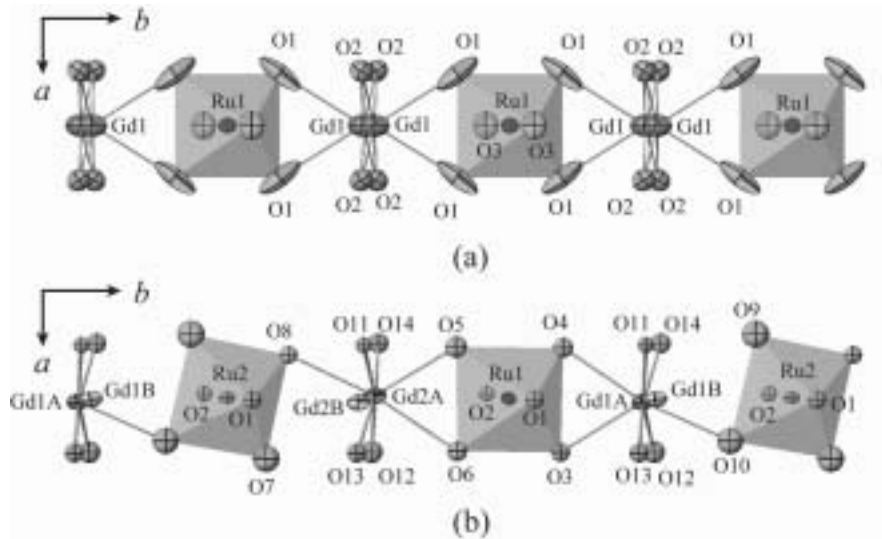


Fig. 9. The $[-\text{Gd-RuO}_6\text{-Gd-RuO}_6\text{-Gd-}]$ linkage in the $Cmcm$ (a) and $P2_1nb$ (b) structures.

half number of octahedra accommodate tilts whereas the remaining half remain untilted. The geometries of (c) and (d) have the antiphase relation against (a) and (b) along the b axis, respectively.

The $Cmcm$ structure can be considered as a superposition of four variants with different geometries. Although each geometry has a doubled periodicity of the $Cmcm$ structure along the b axis, the superposition reduces it into the original value. The O_c atoms are located at the corners of clockwise-tilted, counterclockwise-tilted and untilted octahedra. Superposing all the possible geometries would then make the probability density distribution of O_c rather complicatedly elongated along the arc connecting the octahedral corners. Actually a simple superposition would give rise to a probability density distribution profile composed

of three peaks weighted by 1:2:1 along the arc about the tilt axis. Such distribution is difficult to analyze on the basis of a simple split atom model for O_c . It is also suggested that these four geometries exist in the high-temperature modification not statically but dynamically because the phase transition at 482 K prescribes these geometries to get ordered in the low-temperature modification. In this regard, the $P2_1nb$ - $Cmcm$ phase transition can be considered as an order-disorder transition of the librating $[-\text{Gd-RuO}_6\text{-Gd-RuO}_6\text{-Gd-}]$ linkage along the b axis. This is consistent with the study of the specific heat measurement (Harada & Hinatsu, 2002). The present time-averaged X-ray analysis assumes simple harmonic vibrations for constituent atoms. The prolate feature of O1 ellipsoids thus obtained in the high-temperature modification implies a possible

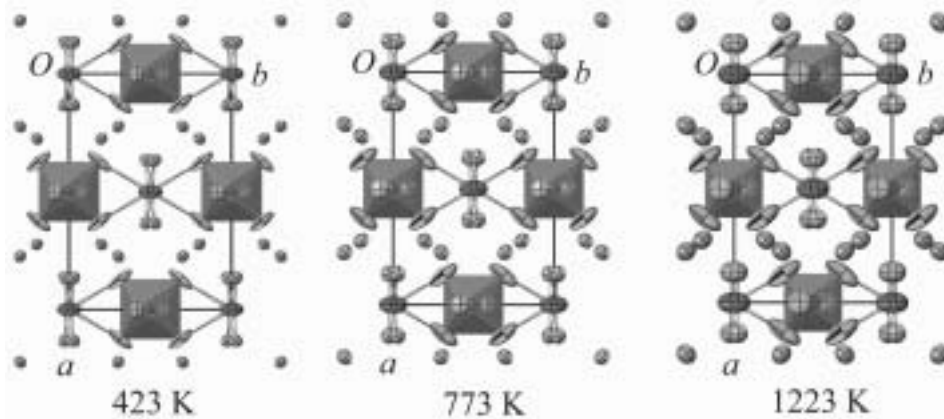


Fig. 10. Changes of the $Cmcm$ structures projected along the c axis as a function of temperature. The anisotropic displacement parameter ellipsoids are plotted at the 97% probability level. The split atom pair of Gd1 (red) is partially overlapped and looks elongated along the b axis in the figure. Four shortest Gd1-O bonds are colored in light blue and the next four in red.

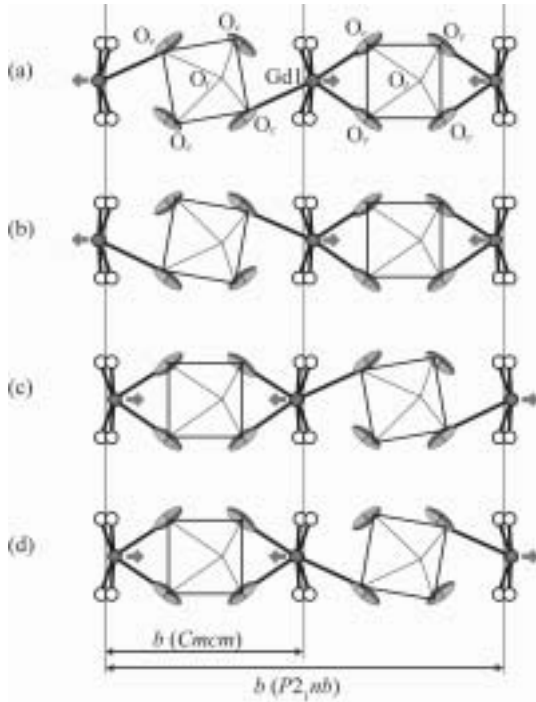


Fig. 11. Four alternative hypothetical structures connecting Gd atoms and $\text{Ru}(\text{O}_c)_4(\text{O}_l)_2$ octahedra along the b axis in the high-temperature form. The Gd1 atom is shown by a circle filled in red with an arrow indicating the direction of its displacement vector from the centre of the split pair. The Gd1-O bonds are drawn by thick solid lines. The original prolate atomic displacement parameter ellipsoids of O1 atoms of the $Cmcm$ modification are superimposed near O_c . Discarded $Cmcm$ model.

presence of complicated dynamical distribution of O_c atoms. The vibrational mode analysis would be a future subject for better understandings of the disorder in the high-temperature modification and the phase transition.

The variants with different displacement models for Gd atoms are also taken into consideration in the earlier stage of the study. Figure 12 illustrates two possible and alternative geometries in the high-temperature modification, in which Gd1 atoms shift in the same direction along b . The periodicity of the geometry is essentially the same as that of the $Cmcm$ modification. All the octahedra have tilts about c with the same sign. The space group becomes $C1c1$ if the direction of Gd1 atom shifts reverses alternately along c . This model, however, contains a flaw in that it includes too short Gd1- O_c distance of around 2.0 Å, as shown by the double line in the figure. The least-squares refinements of the high-form based on the assumption of $C1c1$ were attempted to reproduce the octahedral tilts and the shift mode of Gd1 atoms expected for the model, but failed. The model has been thus discarded.

8. Mechanism of the phase transition

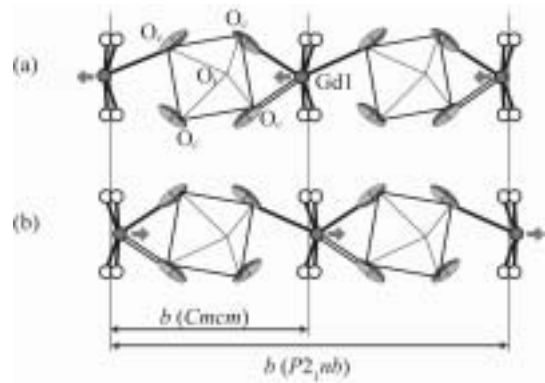


Fig. 12. Two alternative hypothetical structures connecting Gd atoms and $\text{Ru}(\text{O}_c)_4(\text{O}_l)_2$ octahedra along the b axis in the high-temperature form. The Gd1-O bonds are drawn by thick solid lines. The Gd1- O_c distance indicated by double line is approximately 2.0 Å, which is the reason why this model has been discarded. The original prolate atomic displacement parameter ellipsoids of O1 atoms of the $Cmcm$ modification are superimposed near O_c .

The libration of $[-\text{Gd}-\text{RuO}_6-\text{Gd}-\text{RuO}_6-\text{Gd}-]$ linkage which takes place lively in the high-temperature modification should lose energy upon cooling and terminate finally in the low-temperature modification. The termination could be triggered by the dimerization of Ru atoms along the octahedral chain which work effectively to provide an alternatively ordered arrangement of tilted and untilted octahedra along the chain direction. The stoppage of the libration of the $[-\text{Gd}-\text{RuO}_6-\text{Gd}-\text{RuO}_6-\text{Gd}-]$ linkage indicates an order-disorder nature for the transition whereas the dimerization of Ru atoms adds a displacive nature to the transition. These two mechanisms are considered as competitive. The decrease of temperature reduces the libration energy whereas it urges the dimerization of Ru atoms through the electronic interaction.

Below the transition temperature, the symmetry becomes noncentrosymmetric, and has a primitive cell with doubled volume compared with the C -base centered centrosymmetric high-temperature modification. This means that eight possible variants can be brought in the low-temperature crystal, four of which are the antiphase variants of the remainder. Since the high-temperature modification can be considered as a sort of dynamical mixture of four geometries as shown in Fig. 11, inclusion of various variants in the low-temperature modification may be unavoidable.

Actually, a small fraction of Gd atoms was evidenced at the Gd1B and Gd2B sites. The Gd atoms occupy either positions Gd1A or Gd1B with probabilities of approximately 92% and 8%,

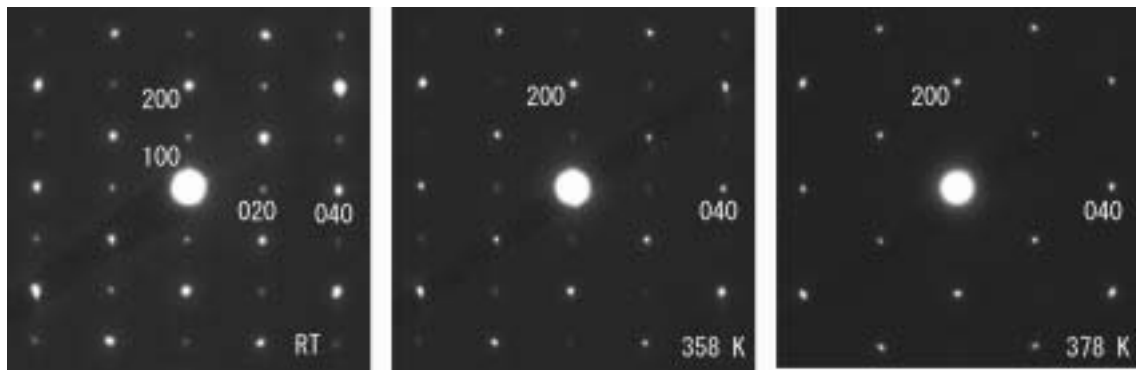


Fig. 13. Changes in the [001] zone axis electron diffraction pattern as a function of temperature. The 100 reflection is probably due to multiple diffraction. Satellite reflections were scarcely observed in this sample.

respectively. The Gd atoms also occupy either positions Gd2A or Gd2B with probabilities of approximately 93% and 7%, respectively. The high correlation between the probabilities of 92-93% at the Gd1A and Gd2A sites suggests a possible coexistence of major variants containing Gd atoms at the A sites and minor variants containing Gd atoms at the B sites in the crystal.

9. Electron diffraction

The *in situ* observation of the electron diffraction pattern was carried out using JEM-2000EX and EM-SHU2 specimen holder (JEOL). The [001] zone axis electron diffraction patterns at room temperature, 358 and 378 K are shown in Fig. 13. Due to presence of the lattice centering in the high-temperature modification, the reflections with $h+k=\text{odd}$ should become extinct. Since the indices in Fig. 13 are given based on the $P2_1nb$ lattice with doubled b -length compared with the high-temperature modification, the extinction rule is

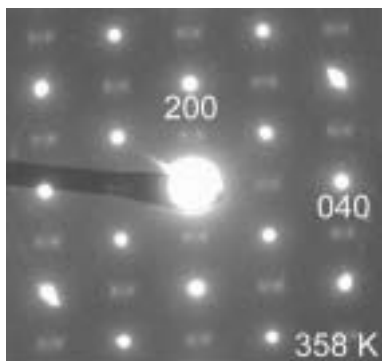


Fig. 14. The [001] zone axis electron diffraction pattern at 358 K. Satellite reflections were clearly observed in many samples.

apparently modified as $h+k/2=\text{odd}$. Actually, the reflections 020, 220, 140, 340, etc., become weak at 358 K and almost disappear at 378 K in Fig. 13. This is consistent with the X-ray diffraction study.

On the other hand, many crystals showed an interesting behavior when they are heated close to the phase transition temperature. A typical [001] zone axis electron diffraction pattern is shown in Fig. 14. The pattern taken at 358 K has diffuse split pairs near the hkl reflections with $h+k/2=\text{odd}$. These satellites align along the b axis at both sides of the reflections with $h+k/2=\text{odd}$. The center reflections with $h+k/2=\text{odd}$ gradually lost their intensity upon heating whereas the satellites became even stronger. The satellites then disappeared suddenly at the transition point and the diffraction pattern changed into that of the high-temperature modification as shown in the rightmost photograph in Fig. 13. The reverse took place upon cooling.

The diffuse split satellites suggest a possible existence of intermediate phase near the phase transition temperature. As discussed in the sections 7 and 8, the transition assumes both properties of the order-disorder and displacive types. If there is a difference in temperature between the two events of termination/initiation of the libration of the $[-\text{Gd}-\text{RuO}_6-\text{Gd}-\text{RuO}_6-\text{Gd}-]$ linkage and the dimerization/dedimerization of the Ru atoms, then an inhomogeneous stress field should appear in the crystal between these events. This could trigger off the intermediate phase.

10. Relation to the other Ln_3RuO_7 compounds

Gemmill *et al.* (2004) reported that the refinement of the $Cmcm$ modifications of Eu_3RuO_7 turned out a poorer fitting than that of Sm_3RuO_7 . The anisotropic atomic displacement parameters of Sm1 and Eu1 atoms in these compounds are approximately 4-times prolate along b , and the values for Eu1 are approximately 50% larger than those for Sm1. This may indicate that the harmonic approximation of a

non-split Ln1 atom model becomes less appropriate for describing the *Cmcm* structure with decreasing ionic radii in the sequence of Ln = Sm³⁺ (4f⁵), Eu³⁺ (4f⁶), and Gd³⁺ (4f⁷).

The *P2₁nb* modifications have been found recently for Ln₃RuO₇ (Ln=Tb³⁺ (4f⁸), Dy³⁺ (4f⁹)) at room temperature. They are also expected to undergo the *P2₁nb-Cmcm* phase transition at high temperatures. If the known phase transition temperatures are plotted against ionic radii of Ln atoms, similar transitions are expected to occur at roughly estimated temperatures of 440 K for Tb₃RuO₇ and 510 K for Dy₃RuO₇. The disorder in the high-temperature modification is also expected for the Tb and Dy compounds, which are subjects of future investigation.

11. Summary

Structural phase transition of trigadolinium ruthenium heptaoxide, Gd₃RuO₇, has been investigated by *in situ* high-temperature X-ray and electron diffraction. A small shrinkage of the *b*-length and an expansion of the *c*-length were observed between 363 and 383 K with increasing temperature. No significant change occurred in *a*-length within experimental errors. The changes were essentially reversible against temperature. Structures of the high-temperature modification have been determined at 423, 773, and 1223 K assuming the orthorhombic *Cmcm* symmetry. The structure of the low-temperature modification has been determined at 293 K, assuming the orthorhombic *P2₁nb* symmetry with doubled unit cell along the *b*-axis of the high-temperature modification. The transition from high- to low-temperature modification can be structurally characterized by tilts about axes close to the *c*-axis occurring on half of the RuO₆ octahedra. These octahedral tilts couple with a reduction in coordination number of the Gd atom bridging the adjacent RuO₆ single chains along the *b*-axis. Dimerization of the Ru array along the chain occurs on the transition, which provides a folding effect on the zigzagging chain in the low-temperature modification. The present study also revealed a presence of structural disorder in the *Cmcm* structure that had not been reported for lanthanide ruthenates (Ln₃RuO₇) and osmates (Ln₃OsO₇) in the literature. The disorder includes a dynamical or static distribution of h-third of Gd atoms in the unit cell, which is presumably linked to the libration of the octahedral tilts about the axes close to *c*. The *P2₁nb-Cmcm* phase transition can

be considered as an order-disorder transition of the librating[-Gd-RuO₆-Gd-RuO₆-Gd-]linkage. Similar phase transitions are expected to occur in Ln₃RuO₇ (Ln=Tb, Dy) with smaller Ln cation sizes at higher temperatures than Gd₃RuO₇. The *in situ* electron diffraction experiments on Gd₃RuO₇ revealed a possible existence of intermediate phase between the high- and low-temperature modifications.

Acknowledgements

This study was supported by Grants-in-Aid for Scientific Research No. 18560662 (HN) and No. 18206071 (NI) from the Japan Society for the Promotion of Science. One of the authors (KT) has been involved in this study as a researcher of the Project Laboratory based on the program of the Ministry of Education, Culture, Sports, Science and Technology “Cooperation for Innovative Technology and Advanced Research in Evolutional Area, West Tounou, Gifu Prefecture”.

References

- Allpress, J. G. ; Rossel, H. J. *J. Solid State Chem.* **1979**, 27, 105-114.
- Bontchev, R. P.; Jacobson, A. J.; Gospodinov, M. M.; Skumryev, V.; Popov, B. Lorenz V. N.; Meng, R. L.; Litvinchuk, A. P.; Iliev, M. N. *Phys. Rev. B.* **2000**, 62, 12235-12240.
- Gemmill, W.R.; Smith, M.D.; zur Loye, H-C. *Inorg Chem.* **2004**, 43, 4254-4261.
- Gemmill, W. R.; Smith, M. D.; Mozharivsky, Y. A.; Miller, G. J.; zur Loye, H-C. *Inorg. Chem.* **2005**, 44, 7047-7055.
- Groen, W. A.; van Berkel, F. P. F.; IJdo, D. J. W. *Acta Cryst.* **1987**, C43, 2262-2264.
- Harada, D.; Hinatsu, Y. *J. Solid State Chem.* **2002**, 164, 163-168.
- Hinatsu, Y.; Wakeshima, M.; Kawabuchi, N.; Taira, N. *J. Alloys Comp.* **2004**, 374, 79-83.
- Ishizawa, N.; Hiraga, K.; du Boulay, D.; Hibino, H.; Ida, T.; Oishi, S. *Acta Cryst. Section E*, **2006**, E62, i13-i16.
- Ishizawa, N.; Tateishi, K.; Kondo S.; Suwa, T. *Inorganic Chemistry* **2007**, 47[2], 558-566.
- Ishizawa, N.; Suwa, T.; Tateishi, K. *Acta Cryst. Sect. E.*, **2007**, E63, i163
- Robinson, K.; Gibbs, G. V.; Ribbe, P. H. *Science* **1971**, 172, 567-570.
- Rossell, H. J. *J. Solid State Chem.* **1979**, 27, 115-122.